Many-Body Theory for Hyperfine Fields in Iron-Group Ions—Ferric Ion*

S. N. Ray, Taesul Lee, and T. P. Das
Department of Physics, State University of New York, Albany, New York 12222
(Received 18 July 1973)

The hyperfine constant of Fe^{+3} ion is calculated by the linked-cluster many-body theory procedure. The first-order contribution representing exchange-core-polarization (ECP) effect leads to a hyperfine constant of -45.46 MHz. Electron-electron interaction effects involving both consistency and correlation contribution are found to be about 12% of the ECP effect. Comparison is made with experimental hyperfine fields in solid state from Mössbauer studies, and the relative importance of covalency effects as compared to electron-electron interaction effects on the hyperfine constant are discussed.

I. INTRODUCTION

The hyperfine interaction in iron-group ions in the solid state is a very interesting property because it gives important information about the nature of the electron distribution in the solid, particularly as it pertains to the extent of the covalent binding in iron-group compounds. To obtain this kind of information it is important to have a knowledge of the free-ion hyperfine constant to determine the difference between the free-ion hyperfine field and that in the solid state. Unfortunately, it has not been possible so far to study experimentally the hyperfine interaction in paramagnetic ions themselves, although measurements have been done[1] in iron-group atoms. One has therefore to rely on theoretical methods to study the hyperfine interactions in free iron-group ions. For this purpose it is desirable to use a method which has proven to be accurate from calculations in atomic systems where experimental hyperfine constants are available. One such method which we intend to follow here is the linked-cluster many-body perturbation-theory (LCMBPT) procedure, which has been applied successfully to the study of the hyperfine constants in a number of atoms—among them alkali atoms,[2] excited states of second-group atoms,[3] and more complicated atoms such as boron,[4] nitrogen,[5] phosphorous,[6] and oxygen.[7] The system we will study in the present work is the ferric ion, both because of the availability of its hyperfine constant in the solid state, from Mössbauer work,[8] and because this is a spherical system where many-body calculations are less cumbersome than for nonspherical systems. One other bonus of this procedure is that it gives the shell-by-shell contributions of both one-electron and many-electron contributions to hyperfine constant which can be related to experimental data which should be obtainable from recently developed techniques involving internal conversion.[9] The exchange-polarization effect is also interesting because of its relationship to energy splitting of different spin states, which has been recently observed through x-ray photoemission technique.[10]

In Sec. II we will briefly discuss the procedure, the choice of the basis set for the evaluation of perturbation diagrams, and a few technical details of the calculation characterizing the ferric ion; we also present the important diagrams that occur in the evaluation of the hyperfine constant and their physical meanings.

Section III will deal with values of the various diagrams and, through their combination, the contributions to the hyperfine constant that one can obtain, namely, from exchange polarization, self-consistency, and correlation effects. A comparison will be made of the one-electron contribution with results from a number of other methods, among them unrestricted Hartree-Fock[11] (UHF), moment perturbation[12] (MP), and exchange polarization[13] (EP). Since Mössbauer data are available in the solid, an analysis will be made of the relationship between the results of our calculation and experimental hyperfine-constant data. Some conclusions are given in Sec. IV.

II. THEORETICAL PROCEDURE

Since the details of the LCMBPT procedure have appeared earlier in the literature,[2-7] we shall present only a few points of the procedure typical of the present system, namely, the type of the potential used, the basis set, and the physical meaning of different diagrams involved. Due to the spherical symmetry of our system, the only relevant hyperfine operator to consider is the contact one.

A. Resumé of LCMBPT

The nonrelativistic total Hamiltonian for an atomic system of N electrons can be written as

$$\mathcal{H} = \sum_{i=1}^{N} T_i + \sum_{i<j} v_{ij} \,, \tag{1}$$

where T_i stands for the sum of the kinetic energy and nuclear Coulomb potential of the ith electron and v_{ij} is the electrostatic interaction between electrons i and j. One needs the exact solution of the Schrödinger equation:

$$\mathcal{H}\Psi_0 = E\Psi_0 \,. \tag{2}$$

In applying the perturbation procedure, we replace

$\mathcal{H}$ by a central field Hamiltonian,

$$\mathcal{H}_0 = \sum_{i=1}^{N} (T_i + V_i) , \tag{3}$$

and $\mathcal{H}' = \mathcal{H} - \mathcal{H}_0$ is treated as a small perturbation. The single-particle potential V_i is selected in such a way that the one-electron equation

$$(T + V)\varphi_i = \epsilon_i \varphi_i \tag{4}$$

is conveniently solvable for a complete set of bound and continuum states having eigenvalues ϵ_i. We have used the restricted Hartree-Fock- (RHF) type V^{N-1} potential for V in Eq. (4), the matrix elements of which are given by[2]

$$\langle a | V^{N-1} | b \rangle = \sum_{n=1}^{N-1} [\langle an | (1/r_{12}) | nb \rangle - \langle an | (1/r_{12}) | bn \rangle] .$$

A normalized zero-order determinantal wave function Φ_0 can be formed out of N of these single-particle states, satisfying the Schrödinger equation

$$\mathcal{H}_0 \Phi_0 = E_0 \Phi_0 . \tag{5}$$

The normalized eigenfunction Ψ_0 can be generated[2] from Φ_0 by using the linked-cluster expansion.[14] The expectation value of an operator O can then be written as

$$\langle O \rangle = \langle \Psi_0 | O | \Psi_0 \rangle = \sum_{n=0}^{\infty} \sum_{m=0}^{\infty} \langle \Phi_0 | [\mathcal{H}'(E_0 - \mathcal{H}_0)^{-1}]^n O [(E_0 - \mathcal{H}_0)^{-1} \mathcal{H}']^m | \Phi_0 \rangle_L , \tag{6}$$

where L indicates that only linked diagrams are to be considered.

B. Basis Set

For the evaluation of the diagrams associated with the perturbation expansion in Eq. (6), one needs a complete set of basis states which are eigenfunctions of the zero-order Hamiltonian $\mathcal{H}_0$.

The complete orthonormal basis set generated by this potential has an infinite number of bound and continuum states. The s, p, and d states were generated in the V^{N-1} potential,[15] with the missing orbital N in Eq. (4) corresponding to a $3s$, $3p$, or $3d$ electron, respectively. For all other excited states, a $3d$ electron was missing. The equations for $P(nl; r)$, which is r times the radial wave functions, are given as follows. For ns states we have

$$\left(\frac{d^2}{dr^2} + \frac{2N}{r} - \frac{1}{r}[Y(r) + 2Y_0(3s^0, 3s^0; r) + 12Y_0(3p^0, 3p^0; r) + 10Y_0(3d^0, 3d^0; r)] + 2\epsilon_{ns}\right) \times P(ns; r) + \frac{2}{r}[Y_0(1s^0, ns; r)P(1s^0; r) + Y_0(2s^0, ns; r)P(2s^0; r) + Y_1(2p^0, ns; r)P(2p^0; r) + Y_1(3p^0, ns; r)P(3p^0; r) + \tfrac{1}{2} Y_2(3d^0, ns; r)P(3d^0; r)] = 0 . \tag{7}$$

For np states we have

$$\left[\frac{d^2}{dr^2} + \frac{2N}{r} - \frac{2}{r^2} - \frac{1}{r}[Y(r) + 4Y_0(3s^0, 3s^0; r) + 10Y_0(3p^0, 3p^0; r) - \tfrac{4}{25} Y_2(3p^0, 3p^0; r) + 10Y_0(3d^0, 3d^0; r)] + 2\epsilon_{np}\right] \times P(np; r) + \frac{2}{r}\{\tfrac{1}{3}[Y_1(1s^0, np; r)P(1s^0; r) + Y_1(2s^0, np; r)P(2s^0; r) + Y_1(3s^0, np; r)P(3s^0; r)] + Y_0(2p^0, np; r)P(2p^0; r) + \tfrac{2}{5} Y_2(2p^0, np; r)P(2p^0; r) + \tfrac{8}{25} Y_2(3p^0, np; r)P(3p^0; r) + \tfrac{1}{3} Y_1(3d^0, np; r)P(3d^0; r) + \tfrac{3}{14} Y_3(3d^0, np; r)P(3d^0; r)\} = 0 . \tag{8}$$

For nd states we have

$$\left[\frac{d^2}{dr^2} + \frac{2N}{r} - \frac{6}{r^2} - \frac{1}{r}[Y(r) + 4Y_0(3s^0, 3s^0; r) + 12Y_0(3p^0, 3p^0; r) + 8Y_0(3d^0, 3d^0; r) - \tfrac{4}{35} Y_2(3d^0, 3d^0; r) - \tfrac{4}{63} Y_4(3d^0, 3d^0; r)] + 2\epsilon_{nd}\right] P(nd; r) + \frac{2}{r}\{\tfrac{1}{5}[Y_2(1s^0, nd; r)P(1s^0; r) + Y_2(2s^0, nd; r)P(2s^0; r) + Y_2(3s^0, nd; r)P(3s^0; r)] + \tfrac{2}{5}[Y_1(2p^0, nd; r)P(2p^0; r) + Y_1(3p^0, nd; r)P(3p^0; r)] + \tfrac{9}{35}[Y_3(2p^0, nd; r)P(2p^0; r) + Y_3(3p^0, nd; r)P(3p^0; r)] + \tfrac{6}{35} Y_2(3d^0, nd; r)P(3d^0; r) + \tfrac{10}{63} Y_4(3d^0, nd; r)P(3d^0; r)\} = 0 . \tag{9}$$

And for nf states we have

$$\left[\frac{d^2}{dr^2}+\frac{2N}{r}-\frac{12}{r^2}-\frac{1}{r}\left[Y(r)+4Y_0(3s^0,3s^0;r)+12Y_0(3p^0,3p^0;r)+8Y_0(3d^0,3d^0;r)\right.\right.$$
$$\left.-\tfrac{4}{45}\,Y_2(3d^0,3d^0;r)-\tfrac{4}{495}\,Y_4(3d^0,3d^0;r)\right]+2\epsilon_{nf}\Big]P(nf;r)+\frac{2}{r}\{\tfrac{1}{7}[Y_3(1s^0,nf;r)P(1s^0;r)$$
$$+Y_3(2s^0,nf;r)P(2s^0;r)+Y_3(3s^0,nf;r)P(3s^0;r)]+\tfrac{9}{35}\,[Y_2(2p^0,nf;r)P(2p^0;r)$$
$$+Y_2(3p^0,nf;r)P(3p^0;r)]+\tfrac{4}{21}\,[Y_4(2p^0,nf;r)P(2p^0;r)+Y_4(3p^0,nf;r)P(3p^0;r)]$$
$$+\tfrac{8}{35}\,Y_1(3d^0,nf;r)P(3d^0;r)+\tfrac{16}{105}\,Y_3(3d^0,nf;r)P(3d^0;r)+\tfrac{160}{847}\,Y_5(3d^0,nf;r)P(3d^0;r)\}=0\,, \tag{10}$$

where

$$Y(r)=4Y_0(1s^0,1s^0;r)+4Y_0(2s^0,2s^0;r)+12Y_0(2p^0,2p^0;r)$$

and

$$Y_k(nl,n'l';r)=r\int_0^\infty \frac{r_<^k}{r_>^{k+1}}P(nl;r')P(n'l';r')\,dr'\,.$$

The normalization procedure is the same as in our earlier paper.[3]

In Eqs. (7)–(10) the core wave functions indicated by superscript 0 refer to those used in the construction of the potential terms. For these, we have used Clementi's RHF wave functions.[16]

C. Description of Hyperfine Operator and Diagrams

As mentioned earlier, the present system is in the ^6S state, and hence only the Fermi-contact part in the hyperfine Hamiltonian exists. The contact Hamiltonian can then be written as

$$\mathcal{H}_c'=\frac{16\pi}{3}\,\frac{\mu_B\mu_N}{Ia_B^3}\,\vec{\mathrm{I}}\cdot\sum_{i=1}^{N}\vec{s}_i\delta(\vec{r}_i)\,. \tag{11}$$

The corresponding spin Hamiltonian is

$$\mathcal{H}'=A\vec{\mathrm{I}}\cdot\vec{\mathrm{J}}\,, \tag{12}$$

where $\vec{\mathrm{I}}$ and $\vec{\mathrm{J}}$ are the spin of nucleus and electronic angular momentum, respectively, and A is the magnetic hyperfine-coupling constant. From Eqs. (11) and (12), A in Hz can be written as

$$A=\frac{8\pi}{3}\left(\frac{\mu_B\mu_N}{IM_Ja_B^3h}\right)\left\langle\Psi(J,M_J)\left|\sum_{i=1}^{N}2s_{z_i}\delta(\vec{r}_i)\right|\Psi(J,M_J)\right\rangle\,. \tag{13}$$

We consider the case where $J=M_J=S=\frac{5}{2}$. To obtain A, one evaluates the expectation value in Eq. (13), which in the LCMBPT formalism is given by Eq. (6), with the operator O being given by $2s_{z_i}\delta(\vec{r})$. To get the value of A in Hz from the individual diagrams which are evaluated in units of a_B^{-3}, it is clear from Eq. (13) that one has to apply the multiplying factor

$$K=\frac{8\pi}{3}\,\frac{\mu_B\mu_N}{IM_Ja_B^3h}\,. \tag{14}$$

Various terms in the perturbation series in Eq. (6) can be obtained by assigning integral values (including 0) to m and n. The terms in this series can be represented by Feynman-like diagrams drawn according to rules described in the LCMBPT literature.[2–7] For these diagrams the hyperfine operator is represented as a wiggly line followed by a letter c. The holes are shown by lines directed down and the particles by lines directed up. A horizontal dotted line corresponds to the electron-electron interaction. The diagrams corresponding to m and n orders in Eq. (6) are referred to as (m, n) diagrams. For example, the $m=0$, $n=1$ diagram in Fig. 1 is referred to as the (0, 1) diagram. Diagrams in Fig. 2 are referred to as (1, 1) diagrams and those shown in Fig. 3 are (0, 2) diagrams. Due to the hermiticity of the operator involved in Eq. (13), the contributions from (m, n) and (n, m) diagrams are equal. Only diagrams surviving after cancellations due to the spin and the potential are shown in Figs. 1–3.

Figure 1 represents the exchange-core-polarization (ECP) effect involving the action of the spin-up valence electron on the core electrons. Diagrams 2(a)–2(f) represent (1, 1) diagrams involving combinations of ECP and one order of electron-electron interaction of the one-electron type. Of these,

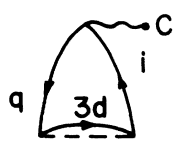

FIG. 1. Exchange-core-polarization diagram.

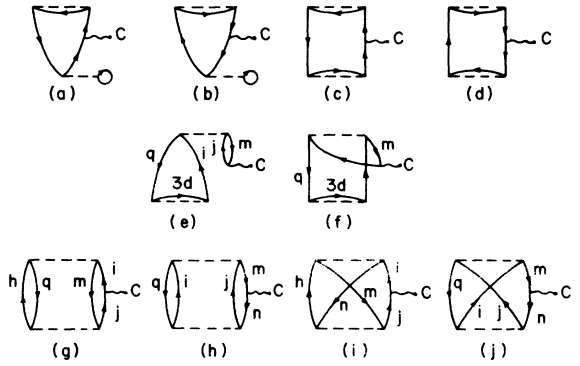

FIG. 2. (1,1) diagrams.

2(a) and 2(b) are combinations of ECP and perturbations which are the result of the use of the V^{N-1} potential. Diagrams 2(c) and 2(d) represent the second order of ECP. Diagrams 2(e) and 2(f) represent the influence of consistency effects on ECP. Diagrams 2(g)–2(j) involve correlation effects in which two electrons are simultaneously excited, 2(i) and 2(j) being, respectively, exchange counterparts of 2(g) and 2(h).

The diagrams in Fig. 3 belong to the (0, 2) category. Diagram 3(a) represents one order in the electron-electron interaction beyond ECP before the contact vertex is applied. For $m=n$, this diagram is referred to as a ladder diagram, which is a consequence of the V^{N-1} potential. Such a diagram does not occur for $m=n=3s$. When $m\neq n$, this diagram represents an indirect ECP effect, one polarized shell influencing the hyperfine contribution from another. For such a diagram n does not have to be an s state. Diagrams 3(b)–3(e) are analogous in physical meaning to diagrams 2(a) and 2(b). Diagrams 3(f) and 3(g) represent higher-order effects associated with ECP and in this respect resemble diagrams 2(c) and 2(d). Diagrams 3(h) and 3(i) like 2(e) and 2(f) represent an interplay of consistency and ECP, while 3(j)–3(m) represent correlation effects.

III. RESULTS AND DISCUSSION

Our results for the various diagrams are presented both with respect to orders of perturbation and to exchange-core-polarization, consistency, and correlation effects. Before considering the results explicitly, we would like to point out a few technical details about the calculation.

The nature of the convergence with respect to l of the particle states observed in the present work and in earlier work on atomic hyperfine interaction indicated that it was sufficient for our work to use up to f states in evaluating the diagrams. For particle states of particular l we included bound states up to principal quantum number $n=10$, while the k values that characterize the continuum states were chosen appropriately to apply a 12-point Gauss-Laguerre integration technique for k space.[3] The conversion factor K in Eq. (14), which converts the values of diagrams in a.u. (a_B^{-3}) to MHz, was calculated[17] to be 28.872.

Our calculation includes all the diagrams up to second order except a few second-order diagrams involving $1s$ hole lines, since we obtained a very small contribution from the $1s$ core to the (0, 1) result.

In Tables I–III, where values of various diagrams are given, superscripts ± are used to indicate the spins associated with the corresponding one-particle states. In these tables, particularly II and III, we have listed individually only the values of those diagrams which contribute more than 0.2 MHz. For the rest of the diagrams, only the net sum is indicated.

We first discuss the (0, 1) results, which correspond to contributions to the ECP effect. The contributions to the (0, 1) diagram of Fig. 1 from various hole states are listed in Table I in the second column. This column is referred to as unladdered to distinguish it from the third column, which involves ladder corrections characteristic of the choice of the potential used. Thus diagrams 3(c), 3(e), and 3(g) with $m=n$ represent hole-hole ladder corrections. For the V^{N-1} potential used here, these diagrams exist only for $m=n=2s$, $1s$ and represent corrections which are a consequence of the difference between the one-electron energies for these states in the V^{N-1} potential and the actual Hartree-Fock energies. Diagram 3(a) with $m=n$

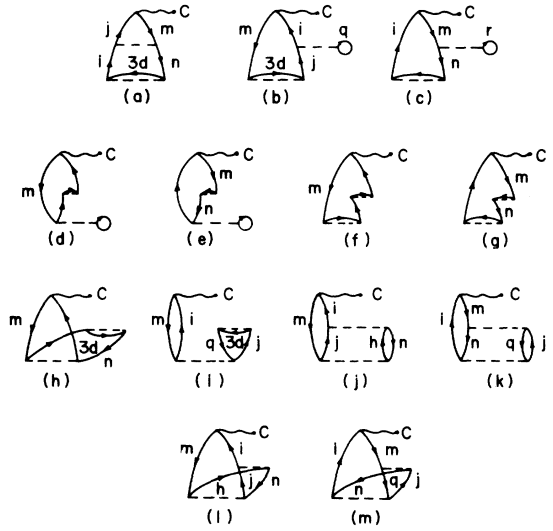

FIG. 3. (0,2) diagrams.

TABLE I. Contributions in MHz from (0,1) diagrams and comparison of the results with other works.

				EP[b]	
q	Unladdered	Laddered	MP[a]	Local Approx.	Corrected for Local Approx.
$1s$	0.103	0.105	0.29	0.29	0.29
$2s$	−47.643	−49.305	−51.50	−49.84	−49.40
$3s$	3.743	3.743	3.56	5.76	3.70
Total	−43.797	−45.457	−45.65	−43.79	−45.41

[a]See Ref. 18. [b]See Ref. 13.

$=2s, 1s$ and 3(b) and 3(f) with $m=2s, 1s$ represent hole-particle ladder diagrams. The influence of these ladder diagrams is incorporated in the third column, the $3s$ contribution being unaffected by ladder effects, since there are no ladder diagrams involving the $3s$ hole state for the choice of the V^{N-1} potential made in this work. We have compared the shell-by-shell contributions from the (0, 1) diagrams with other perturbation approaches. Thus the fourth column lists the state-by-state contribution obtained by the moment-perturbation procedure,[18] involving the calculation of perturbations of the core states by the nuclear hyperfine interaction. The fifth column gives corresponding results by the exchange-perturbation procedure,[13] involving perturbed wave functions for the cores due to the exchange potential produced by the $3d$ electrons. For the results in both the fourth and fifth columns, a local approximation devised by Sternheimer[19] was employed. The sixth column includes corrections due to the difference between the local approximation and the nonlocal Hartree-Fock potential. Comparing the fifth and sixth columns, the influence of the nonlocal potential correction is seen to be most significant for the outermost-core $3s$ states, as one would expect since these are the least bound of all the cores. The agreement, shell by shell between the (0, 1) results and the MP and EP results, is very good in spite of the fact that these latter perturbation procedures involve totally different techniques from the LCMBPT procedure employed here. It is interesting that the incorporation of nonlocal effects improves the agreement between the EP and our results for the $3s$ state. One might expect a similar trend for the MP case on incorporating nonlocal effects, improving its agreement with the LCMBPT result.

The contributions from the (1, 1) diagrams are listed in Table II. We have listed the results of consistency diagrams and pure correlation diagrams separately. The consistency effect receives comparable contributions from diagrams involving both $3s$ and $2s$ states. While $3s$ states are more deformable, the $2s$ states have greater density at the nucleus, which leads to the comparable nature of their contributions. A similar remark applies to correlation effects from $2s$ and $3s$ states. The net (1, 1) contribution of 1.655 MHz is comprised of 0.621 MHz from consistency and 1.034 MHz from correlation effects.

Table III presents the contributions from (0, 2) diagrams, excluding those diagrams referring to laddering effects which were included in Table I. Of the two consistency diagrams 3(a) and 3(h), 3(a)

TABLE II. Contributions from (1,1) diagrams shown in Figs. 2(a)–2(j).

Diagram	Excitation	Contribution in MHz
	Consistency	
2(a)–2(d)		−0.009
2(e)	$q=3s^{+}$ $m=3s^{-}$	0.241
	$q=2s^{+}$ $m=2s^{-}$	−0.241
2(f)	$q=3p$ $m=3s$	0.714
	$q=3p$ $m=2s$	0.232
	$q=2p$ $m=2s$	−0.378
Other Consistency Diagrams		0.062
Total Consistency Contribution		0.621
	Correlation	
2(g)	$q=3p$ $m=3d$	0.660
2(h)	$q=3p$ $m=n=3s^{-}$	2.894
	$q=3p$ $m=3s^{-}$ $n=2s^{-}$	−1.238
	$q=3p$ $m=n=2s^{-}$	0.222
	$q=3d$ $m=n=3s^{-}$	0.385
	$q=3d$ $m=3s^{-}$ $n=2s^{-}$	−0.203
2(i)	$n=3p$ $m=3d$	−1.068
	$n=3d$ $m=3s$	−1.063
2(j)	$q=3p$ $m=n=3s^{-}$	−1.987
	$q=3p$ $m=3s^{-}$ $n=2s^{-}$	0.767
	$q=3p$ $m=n=2s^{-}$	−0.205
	$q=3d$ $m=n=3s$	1.952
	$q=3d$ $m=3s$ $n=2s$	−0.912
	$q=3d$ $m=2s$ $n=2s$	0.325
Other Correlation Diagrams		0.505
Total Correlation		1.034
Net (1,1) Contribution		1.655

TABLE III. Contributions from (0,2) diagrams shown in Figs. 3(a)–3(m).

Diagram	Excitation			Contribution in MHz
	Consistency			
3(a)	$m=3s$	$n=3p$		3.695
	$m=1s$	$n=2s$		−0.234
	$m=3s$	$n=2s$		−0.243
	$m=1s$	$n=3p$		−0.322
	$m=1s$	$n=2p$		0.723
	$m=2s$	$n=2p$		−1.875
3(h)	$m=3s$	$n=3p$		0.457
	$m=2s$	$n=2p$		−0.215
Other Consistency Diagrams				+0.283
Total Consistency Contribution				2.269
	Correlation			
3(j)		$m=3s$	$n=3d$	−0.546
		$m=3s$	$n=2p$	−0.384
3(k)	$q=3s$	$m=3s$	$n=3d$	−0.758
	$q=3p$	$m=3s$	$n=3p$	−2.500
	$q=3p$	$m=3s$	$n=3d$	−0.610
	$q=2s$	$m=2s$	$n=3d$	0.453
	$q=2p^-$	$m=3s^+$	$n=2p^+$	0.388
	$q=2p^-$	$m=2s^+$	$n=2p^+$	0.224
	$q=3p^-$	$m=2s^+$	$n=3p^+$	−1.029
	$q=2p$	$m=3s$	$n=3d$	−0.347
	$q=3p$	$m=2s$	$n=3d$	0.482
	$q=2p$	$m=2s$	$n=3d$	0.366
3(l)		$m=3s$	$n=3p$	1.016
		$m=3s$	$n=3d$	−3.493
		$m=3s$	$n=2p$	0.499
		$m=2s^-$	$n=3p^-$	−0.375
		$m=2s^-$	$n=2p^-$	−0.348
		$m=2s$	$n=3d$	1.754
3(m)	$q=3d$	$m=3s$	$n=3s$	1.072
	$q=3s$	$m=3s$	$n=3d$	2.369
	$q=3p$	$m=3s$	$n=3d$	0.430
	$q=3d$	$m=3s$	$n=3p$	1.204
	$q=3d$	$m=2s$	$n=3s$	−0.304
	$q=2s$	$m=2s$	$n=3d$	−1.018
	$q=2p$	$m=2s$	$n=3d$	−0.633
	$q=3d$	$m=2s$	$n=3p$	−0.469
	$q=3p^-$	$m=3s^-$	$n=2p^-$	1.184
	$q=2p^-$	$m=3s^-$	$n=3p^-$	1.615
	$q=3p^-$	$m=2s$	$n=2p^-$	0.901
	$q=2p^-$	$m=2s^-$	$n=3p^-$	1.018
Other Correlation Diagrams				0.184
Total Correlation Contribution				2.295
Net (0,2) Contribution				4.564

is the major contributor and can be physically interpreted as representing an indirect ECP effect. Thus one could analyze this diagram as an exchange perturbation of hole state n by the unpaired $3d$ electrons; the exchange-polarized n state then further perturbs state m, which later then leads to a finite spin density at the nucleus. Of the various combinations of m and n states which contribute to this indirect ECP diagram, the one involving $m=3s$ and $n=3p$ is seen to be the most effective. This is understandable, because both $3d$-$3p$ and $3p$-$3s$ exchange interactions are strong. The $n=2p$, $m=2s$ combination is also important, because the $2p$-$2s$ exchange is strong and the $2s$ state has a large amplitude at the origin. It is also interesting that some of the indirect ECP diagrams involving 1s make small but significant contributions and, in fact, stronger contributions than the direct ECP diagram in Fig. 1. The reason for this is that, while $1s$ exchanges rather weakly with $3d$, it interacts more strongly with the other core states, which can then communicate by exchange with the $3d$ electrons.

The (0, 2) correlation diagrams are seen from Table III to consist of a number of contributions of comparable magnitude with considerable cancellations due to differing signs. The diagrams with largest magnitudes are seen to arise from interactions involving $3d$, $3p$, and $3s$ states, which correlate most strongly. Diagrams involving $2s$ states in this order are important only when a hyperfine vertex is attached to $2s$ and takes advantage of the relatively large amplitude of $2s$ state at the nucleus.

In Table IV the net contributions from the various orders are summarized together with separation into different physical effects: ECP, consistency, and correlation, as in Tables I–III. The net contributions from consistency and correlation are comparable, as indeed are the individual ones for both (1, 1) and (0, 2) orders. On combining the net consistency and ECP effects, one gets a net one-electron result for $A=-42.57$ MHz. For the EP calculation discussed earlier,[13] indirect ECP effects have also been evaluated, and their inclusion leads to $A=-41.04$ MHz, which is in reasonable agreement with our one-electron results. Two UHF calculations have been carried out, one involving a Slater-type basis set[11] and one a Gaussian.[20] The results from these calculations are, respectively, −34.58 and −43.59 MHz. On including correlation effects, our calculation leads to a net hyperfine constant for the free ion given by $A=-39.2$ MHz or −711.9 kOe in units of field at the nucleus. An error limit of ±0.5 MHz could be added to this result due to the numerical inaccuracy, neglect of some diagrams (as pointed out earlier), and higher angular momentum components. It is hoped that in the future results will be available for the free Fe^{+3} ion or the ion trapped in a weakly interacting environment, such as a rare-gas solid, to directly compare with our theoretical result. For the present, we can only use our result for A for the free ion as a reference to compare with the values of A in solid-state compounds to obtain the solid-state effect on A. Thus, using recent tabulations of Fe^{57} hyperfine-field data[21] in K_2NaFeF_6,

TABLE IV. Summary of contributions to hyperfine constant (in MHz).

(0,1)	(1,1)		(0,2)				
ECP	Consistency	Correlation	Consistency	Correlation	Net Consistency	Net Correlation	Total
−45.457	0.621	1.034	2.269	2.295	2.890	3.329	−39.238

$\gamma - Fe_2O_3$, and $FeCl_3$, our free-ion hyperfine result leads to +91.9, +196.9, and +243.9 kOe, respectively, from the influence of solid-state effects. In a recent calculation[22] on the Mn^{+2} ion in ZnF_2, the influence of overlap effects was seen to lead to a contribution of 23% of the free-ion magnitude, but with positive sign. The recent UHF calculation[20] on K_3FeF_6 using Gaussian orbitals has led to +42 kOe from valence orbitals. It is not our aim here to analyze the accuracy of solid-state calculations. We can remark, however, that both the above results are in the right direction and have the right order of magnitude to explain the differences between solid-state free-ion hyperfine fields. More solid-state calculations, especially in the three systems listed earlier, would be helpful in understanding the influence of neighboring ions in the solid.

IV. CONCLUSIONS

We conclude by listing a number of conclusions that may be drawn from the present calculations and earlier work on Mn^{++} ion: (a) Consistency and correlation effects within the ion are an order of magnitude smaller than the ECP effect. (b) However, for the study of solid-state effects using the free-ion hyperfine constant as reference, consistency and correlation effects are very important, because from Table IV they are seen to be of the same order of magnitude. (c) For the study of ECP effects from individual shells by techniques such as internal conversion,[9] consistency and correlation effects are relatively important, since they are comparable to ECP for the 3s shell.

*Supported by National Science Foundation.

[1]W. J. Childs and L. S. Goodman, Phys. Rev. **148**, 74 (1966).
[2]Edward S. Chang, Robert T. Pu, and T. P. Das, Phys. Rev. **174**, 1 (1968); T. Lee, N. C. Dutta, and T. P. Das, Phys. Rev. A **1**, 995 (1970).
[3]S. N. Ray, Taesul Lee, and T. P. Das, Phys. Rev. A **7**, 1469 (1973).
[4]J. E. Rodgers and T. P. Das (unpublished).
[5]N. C. Dutta, C. Matsubara, R. T. Pu, and T. P. Das, Phys. Rev. **177**, 33 (1969).
[6]N. C. Dutta, C. Matsubara, R. T. Pu, and T. P. Das, Phys. Rev. Lett. **21**, 1139 (1968).
[7]Hugh P. Kelly, Phys. Rev. **173**, 142 (1968).
[8]G. Ziebarth, Z. Phys. **212**, 330 (1968) and also see Ref. 21.
[9]Cheng-jyi Song, Jan Trooster, N. Benczer-Koller, and G. M. Rothberg, Phys. Rev. Lett. **29**, 1165 (1972).
[10]R. L. Cohen, G. K. Wertheim, A. Rosencwaig, and H. L. Guggenheim, Phys. Rev. B **5**, 1037 (1972).
[11]R. E. Watson and A. J. Freeman, Phys. Rev. **123**, 2027 (1961).
[12]L. Tterlikkis, S. D. Mahanti, and T. P. Das, Phys. Rev. **176**, 10 (1968).
[13]K. J. Duff and T. P. Das, Phys. Rev. **168**, 43 (1968).
[14]J. Goldstone, Proc. R. Soc. A **239**, 267 (1957); K. A. Brueckner, Phys. Rev. **97**, 1353 (1955); Phys. Rev. **100**, 36 (1955).
[15]Hugh P. Kelly, Phys. Rev. **136**, B896 (1964).
[16]E. Clementi, IBM J. Res. Dev. **9**, 2 (1965).
[17]B. N. Taylor, W. H. Parker, and D. N. Langenberg, Rev. Mod. Phys. **41**, 375 (1969); *N. M. R. Table*, 5th ed. (Varian, New York, 1965).
[18]R. M. Sternheimer, Phys. Rev. **93**, 734 (1956).
[19]Dennis Ikenberry (private communication).
[20]K. J. Duff (unpublished).
[21]S. Hüfner and G. K. Wertheim, Phys. Rev. B **7**, 2333 (1973).
[22]D. Ikenberry and T. P. Das, Phys. Rev. B **2**, 1219 (1970).